ChemComm

COMMUNICATION

Electrochemistry of Au^{II} and Au^{III} pincer complexes: determination of the Au^{II}–Au^{II} bond energy†

Thomas Dann, Dragoş-Adrian Roşca, Joseph A. Wright,* Gregory G. Wildgoose* and Manfred Bochmann*

The bond energy of the unsupported Au–Au bond in the Au(II) dimer [(C^N^C)Au]$_2$ and the difference between Au^{III}–OH and Au^{III}–H bond enthalpies have been determined experimentally by electrochemical methods, with Au–OH and Au–H complexes showing unexpected differences in their reduction pathways, supported by DFT modelling.

The chemistry of gold complexes is dominated by compounds in oxidation states I and III.[1] There are comparatively few Au(II) complexes, and most of these possess a binuclear Au^{II}–Au^{II} core supported by bridging ligands. Without such ligands Au(II) has a tendency to disproportionate into Au(I) and Au(III).[2,3] There are only few examples of compounds which contain an unsupported Au^{II}–Au^{II} bond.[4–7] Zopes *et al.* recently reported the formation of $[Au^{II}(CF_3)_2(py)]_2$,[6] and Xiong and Pyykkö suggested a $6s5d_{xy}6p_z$-type hybridization for the Au–Au bond and calculated an Au–Au bond energy of about 200 kJ mol^{-1}, depending on the ligands.[8] $[Au^{II}(CF_3)_2(py)]_2$ spontaneously disproportionates in solution into Au(I) and Au(III) products.[6] By contrast, we have recently shown that the Au(III) pincer complexes (C^N^C)AuOH (**1**)[9] and (C^N^C)AuH (**2**) undergo reductive condensation to give the temperature- and air-stable Au(II) complex **4** (eqn (1)).[7] This unusual stability caused us to investigate the bonding in this compound in more detail and to determine the Au–Au bond energy by electrochemical and computational methods. Unsupported Au–Au bonds show significant variations in metal–metal distances (and therefore Au–Au bond energies), ranging from 2.6405(8) Å in [{Au(dppn)I}$_2$]-(PF$_6$)$_2$[4b] to 2.5062(9) Å in [Au(CF$_3$)$_2$(py)]$_2$[6] (py = pyridine; dppn = 1,8-bis(diphenylphosphino)naphthalene).

We report here the voltammetric characterisation of the Au(III) pincer complexes (C^N^C)AuH **1**, (C^N^C)AuOH **2**, and (C^N^C)-AuCl, **3**[10] and the Au(II) complex **4**, together with digital simulations of the recorded voltammetry to yield globally optimised parameters for the electrochemistry describing the kinetic and thermodynamic

*Wolfson Materials and Catalysis Centre, School of Chemistry, University of East Anglia, Norwich, NR4 7TJ, UK. E-mail: m.bochmann@uea.ac.uk;
Fax: +44 (0)16035 92044*
† Electronic supplementary information (ESI) available: Electrochemistry and digital simulation of cyclic voltammetry details, computational details. See DOI: 10.1039/c3cc45984e

$$(1)$$
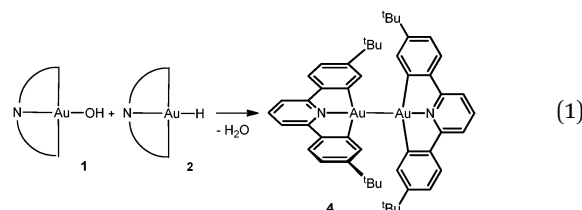
redox properties of these complexes.[11,12] The thermodynamic data gleaned from the digital simulation of the voltammetric data alongside DFT calculations are used to estimate the Au^{II}–Au^{II} bond strength and to rationalise the unusual reactivity and chemistry of (C^N^C)Au^{II}X complexes (X = H or OH).

The direct cyclic voltammetric characterisation of the gold pincer complexes **1**–**4** was carried out in CH$_2$Cl$_2$ using 0.1 M [NBu$_4$][B(C$_6$F$_5$)$_4$] as supporting electrolyte. Initially survey scans were obtained by first scanning from potentials where no Faradaic current flows in a reductive direction to the edge of the solvent window before reversing the potential up to the oxidative edge of the solvent window at a scan rate of 100 mV s^{-1} (Fig. 1).

In the case of **1** two reduction waves are observed with peak potentials at −2.39 and −2.66 V *vs.* Fc$^{0/+}$ respectively.[13] In these survey scans no corresponding oxidation waves are observed upon reversing the scan direction either at the reductive limit of solvent breakdown or sequentially after passing each reduction peak potential. This suggests that the reduction waves correspond to either electrochemically or chemically irreversible processes. An irreversible
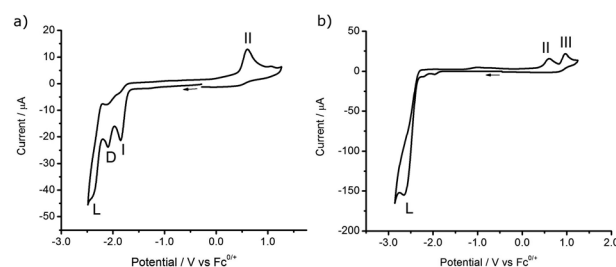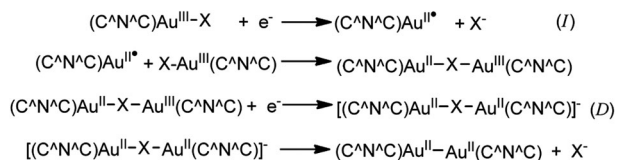

Fig. 1 Full range cyclic voltammograms of **3** (a) and **4** (b) in CH$_2$Cl$_2$ (1.5 mM, 0.05 M [nBu$_4$N][B(C$_6$F$_5$)$_4$]) at a scan rate of 100 mV s^{-1}.

$$(C^\wedge N^\wedge C)Au^{III}\text{-}X \ + \ e^- \longrightarrow (C^\wedge N^\wedge C)Au^{II\bullet} \ + \ X^- \qquad (I)$$

$$(C^\wedge N^\wedge C)Au^{II\bullet} + X\text{-}Au^{III}(C^\wedge N^\wedge C) \longrightarrow (C^\wedge N^\wedge C)Au^{II}\text{-}X\text{-}Au^{III}(C^\wedge N^\wedge C)$$

$$(C^\wedge N^\wedge C)Au^{II}\text{-}X\text{-}Au^{III}(C^\wedge N^\wedge C) + e^- \longrightarrow [(C^\wedge N^\wedge C)Au^{II}\text{-}X\text{-}Au^{II}(C^\wedge N^\wedge C)]^- \quad (D)$$

$$[(C^\wedge N^\wedge C)Au^{II}\text{-}X\text{-}Au^{II}(C^\wedge N^\wedge C)]^- \longrightarrow (C^\wedge N^\wedge C)Au^{II}\text{-}Au^{II}(C^\wedge N^\wedge C) + X^-$$

Scheme 1 Electron transfer steps for the reduction steps I and D; X = H, Cl.

oxidation wave is observed at +0.59 V vs. Fc$^{0/+}$, but only when the potential was first scanned to more negative potentials than that of the first reduction wave at −2.39 V. By comparison with the voltammetry of the dimeric [(C$^\wedge$N$^\wedge$C)Au^{II}]$_2$ (4) we can assign the oxidation wave at +0.59 V to be the oxidation of 4, which we postulate is formed as a product of the initial reduction of 1 at −2.39 V. Hence we assign the first reduction wave to the reduction of the Au^{III} metal centre. By comparison with the voltammetry of structurally related alkynyl Au^{III} pincer complexes reported by Yam et al.[10,11] the large, irreversible reduction wave at −2.66 V vs. Fc$^{0/+}$ (labelled L) may be attributed to a complex multi-electron ligand-based reduction process and will not be considered further.

In the case of LAu^{III}H (2) three reduction waves are observed with peak potentials at −2.00 V (corresponding to a metal centred Au(III → II) reduction, labelled I), −2.25 V and −2.60 V vs. Fc$^{0/+}$, respectively. We assign the −2.25 V wave (labelled D in Scheme 1 and Fig. 1) tentatively to the reduction of a bridged complex of the type [(C$^\wedge$N$^\wedge$C)Au^{II}–H–Au^{III}(C$^\wedge$N$^\wedge$C)] formed from the reaction of 2 with a (C$^\wedge$N$^\wedge$C)Au^{II} radical. Such an intermediate is only observed for the hydride 2 and chloride 3, but not for the hydroxide 1. The third reduction at −2.60 V (labelled L in Scheme 1 and Fig. 1) again corresponds to ligand based multi-electron processes. As was the case with 1, no corresponding oxidation waves are seen upon reversing the scan direction from the solvent window or sequentially after each reduction potential, indicating that each reduction exhibits electrochemically or chemically irreversible behaviour. The same irreversible oxidation wave at +0.59 V vs. Fc$^{0/+}$ is observed with 2 as it was with 1, and again this oxidation wave is only observed after first scanning the potential beyond the reduction wave at −2.25 V, supporting our assignment of a metal-centred Au(III → II) reduction with subsequent dimerisation of the (C$^\wedge$N$^\wedge$C)Au^{II} radical intermediates to form 4 (Scheme 1).

(C$^\wedge$N$^\wedge$C)Au^{III}Cl 3 was characterised by voltammetry as a control to account for the possibility of halogen abstraction from the CH$_2$Cl$_2$ solvent. We observed similar voltammetry to 2, with three reductions at −1.85, −2.10 and −2.45 V vs. Fc$^{0/+}$, respectively (Fig. 1a). The first is assigned to reduction step I, the second to D, the third to the ligand based reduction L.

The dimer 4 shows the ligand reduction at −2.63 V vs. Fc$^{0/+}$, as well as an irreversible oxidation wave at +0.59 V vs. Fc$^{0/+}$, due to the direct oxidation of 4 at the electrode (Fig. 1b). A second oxidation wave (labeled III) is also observed at +0.97 V vs. Fc$^{0/+}$, that is not seen in the case of 1 or 2, which only appears after the ligand-based reduction (L) has occurred. We therefore assign this to the oxidation product of ligand decomposition.

To further investigate the electrochemical behaviour of 1–4, cyclic voltammetry was performed at varying scan rates from 50 to 1000 mV s^{-1}. In the case of 1, at scan rates >100 mV s^{-1} a corresponding re-oxidation wave for the metal-centred reduction

at −2.39 V vs. Fc$^{0/+}$ becomes apparent. This suggests that in the electrochemical reduction of 1 the initial heterogeneous electron transfer is quasi-reversible but is followed by an irreversible, homogeneous chemical step involving the cleavage of the Au–OH bond and subsequent dimerisation of the (C$^\wedge$N$^\wedge$C)Au^{II} radical (EC mechanism using Testa–Reinmuth notation[14]). As the voltage scan rate is increased, the kinetics of the follow-up chemical step(s) begin to be outrun on the voltammetric timescale, such that some – but not all – of the Au(II) intermediate is subsequently re-oxidized to the parent LAu^{III}OH complex before the Au–OH bond is cleaved and dimerisation can occur. The fact that the dimer oxidation wave at +0.59 V is still observed at all scan rates indicates that some of the LAu^{II} intermediates are still able to dimerise even at the higher scan rate of 1 V s^{-1}.

The behaviour of 1 is in contrast to that of the hydride 2, in which no back-peak corresponding to the initial metal-centred reduction is observed at any scan rate up to 1 V s^{-1}. This suggests that the Au^{II}–H bond is broken more rapidly than the Au^{II}–OH bond, such that any follow-up homogenous chemical step(s) are not being outrun on the voltammetric timescale (up to scan rates of 1 V s^{-1}). The faster cleavage of the Au^{II}–H compared to Au^{II}–OH contrasts with the bond energies of the parent Au^{III}–X compounds, where the Au^{III}–OH bond was calculated to be weaker than the Au^{III}–H bond (279 vs. 317 kJ mol^{-1}).[15]

This may be explained by different reduction pathways for the two species. DFT calculations show that for X = H (Scheme 1) the reaction of [(C$^\wedge$N$^\wedge$C)Au^{III}–X] with a (C$^\wedge$N$^\wedge$C)Au^{II} fragment to give a [(C$^\wedge$N$^\wedge$C)Au–X–Au(C$^\wedge$N$^\wedge$C)] intermediate is exothermic by 49 kJ mol^{-1}. This species has a roughly symmetrical Au–H–Au core which is retained on reduction. In contrast, when X = OH no OH-bridged molecular intermediate could be identified: the second gold fragment associates only weakly with the oxygen atom (Au···O distance 2.487 Å).

In all cases the oxidation of 4 (+0.59 V vs. Fc$^{0/+}$) is irreversible at all voltage scan rates. This would suggest that the product of the oxidation of the Au(II) dimer is unstable and likely undergoes rapid follow-up chemistry, probably involving cleavage of the Au^{II}–Au^{II} bond to form redox inactive products. There was no evidence for detectable amounts of a mixed-valence radical cation intermediate [(C$^\wedge$N$^\wedge$C)Au^{II}–Au^{III}(C$^\wedge$N$^\wedge$C)]$^+$ in the oxidation process.

Digital simulations of the metal centred reductions of 1 and 2 and the oxidation of 4 provided kinetic and thermodynamic parameters and support for the mechanisms of the observed electrochemical processes. The best fit between experiment and theory (Fig. 2) is consistent with the mechanisms discussed above, where the Au(III) centres each undergo a one-electron reduction concomitant with Au–X bond cleavage (X = H$^-$ or OH$^-$) at the electrode (E-step), followed by rapid dimerisation between two (C$^\wedge$N$^\wedge$C)Au^{II} radicals (C-step). This dimer 4 can then undergo a one-electron oxidation (E-step) at more positive potentials. The identity of the product of this oxidation is currently unknown but, given the irreversible nature of the oxidation, we postulate that it likely involves cleavage of the Au^{II}–Au^{II} bond. As we found earlier,[7] (C$^\wedge$N$^\wedge$C)Au^{II} pincer complexes are resistant to disproportionation, and any mechanism involving a disproportionation step gave poor fits between experiment and simulation and were thus discounted. The overall mechanism can therefore be described as ECEC, in
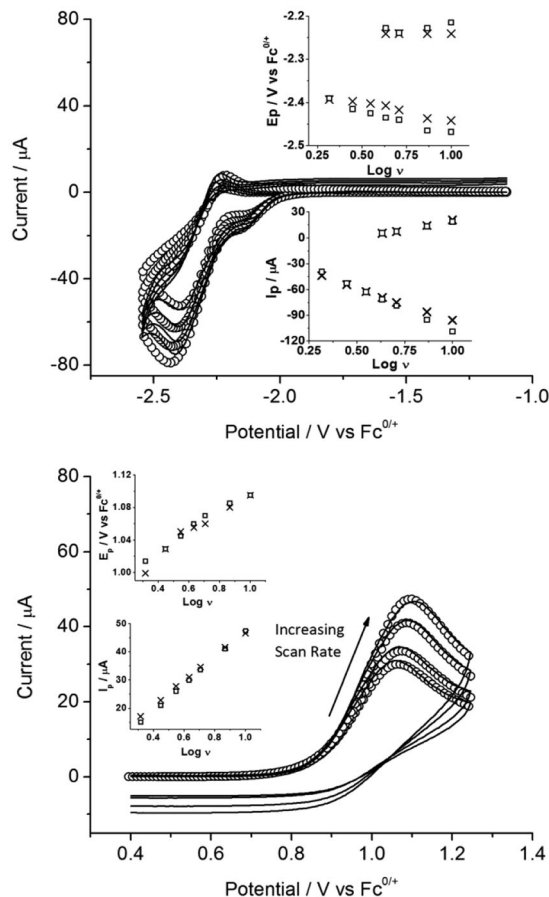
Fig. 2 Experimental (solid line) and simulated (open circles) overlaid cyclic voltammograms of **1** (top), **4** (bottom), (all redox active species initially present at 1.5 mM; 0.05 M [nBu$_4$N][B(C$_6$F$_5$)$_4$] supporting electrolyte) at scan rates of 200–500 mV s^{-1}. Inset: plots comparing simulated (open squares) and experimental (crosses) peak potentials (E_p) and peak currents (I_p).

Table 1 Simulated electrochemical parameters for the reduction of **1** and **2** and oxidation of **4**

Parameter	LAuOH (**1**)	LAuH (**2**)	LAu–AuL (**4**)
E^0/V $vs.$ Fc$^{0/+}$	−2.30	−1.91	0.60
α	0.3	0.35	0.6
k^0/10^{-3} cm s^{-1}	5.4 ± 0.5	2.0 ± 0.1	68 ± 0.2
D_0/10^{-5} cm^2 s^{-1}	1.51 ± 0.1	1.60 ± 0.1	0.70 ± 0.1

which the chemical step is a bimolecular dimerisation. Table 1 summarises the globally optimised parameters for the metal-centred reduction of **1** and **2** and oxidation of **4** (formal potential, E_f^0; charge transfer coefficient, α; standard electron transfer rate constant, k^0; diffusion coefficient, D_0).[16]

The Au^{II}–Au^{II} bond energy of **4**, along with Au–H/OH bond energy difference between **1** and **2** were estimated using the formal potentials obtained above (corrected to the standard hydrogen electrode, SHE; the minor difference between formal and standard potential, E^0, which accounts for non-ideality in activities, is neglected and is likely within the error range reported). Neglecting entropic contributions, the Au^{II}–Au^{II} bond enthalpy is estimated to be 198 ± 1 kJ mol^{-1}. This value

is in good agreement with the bond energy of **4** calculated by DFT methods, 225 kJ mol^{-1}, and the value of approximately 200 kJ mol^{-1} recently calculated by Xiong and Pyykkö[8] for structurally similar [Au^{II}X$_2$(py)]$_2$ complexes. If we neglect differences in solvation between hydride and hydroxide ions, then a similar Hess cycle can be used to estimate the difference between the Au–OH and Au–H bond enthalpy, which shows that the Au^{III}–H bond is more stable by $ca.$ 19 kJ mol^{-1}. This value is reassuringly similar to that predicted by our DFT calculations.[15]

The Au(II) dimer **4** is air stable and does not insert O$_2$ into the Au–Au bond, even though the reaction **4** + O$_2$ → (C^N^C)Au–OO–Au(C^N^C) is exothermic by 136 kJ mol^{-1} and the resulting peroxide product is accessible by other routes.[15] It is stable to disproportionation under thermal conditions.

In summary, we have reported the first experimental determination of the bond energy of an unsupported Au^{II}–Au^{II} bond. The value is in agreement with DFT calculations, as are the relative Au^{III}–H and Au^{III}–OH bond energies. The electrochemical reduction pathway of (C^N^C)Au^{III}–X pincer complexes shows unexpected differences, with X = H proceeding via a bridged intermediate, whereas X = OH does not.

Notes and references

1 M. C. Gimeno and A. Laguna, in *Comprehensive Coordination Chemistry II*, ed. J. A. McCleverty and T. J. Meyer, Elsevier, Amsterdam, 2003, vol. 6, pp. 911–1145.
2 (*a*) A. Laguna and M. Laguna, *Coord. Chem. Rev.*, 1999, **193–195**, 837; (*b*) A. A. Mohamed, H. E. Abou and J. P. Fackler Jr, *Coord. Chem. Rev.*, 2010, **254**, 1253.
3 E. Tkatchouk, N. P. Mankad, D. Benitez, W. A. Goddard III and F. D. Toste, *J. Am. Chem. Soc.*, 2011, **133**, 14293.
4 (*a*) V. W.-W. Yam, S. W.-K. Choi and K.-K. Cheung, *J. Chem. Soc., Chem. Commun.*, 1996, 1173; (*b*) V. W.-W. Yam, C.-K. Li, C.-L. Chan and K.-K. Cheung, *Inorg. Chem.*, 2001, **40**, 7054.
5 J. Coetzee, W. F. Gabrielli, K. Coetzee, O. Schuster, S. D. Nogai, S. Cronje and H. G. Raubenheimer, *Angew. Chem., Int. Ed.*, 2007, **46**, 2497.
6 D. Zopes, C. Hegemann, W. Tyrra and S. Mathur, *Chem. Commun.*, 2012, **48**, 8805.
7 D.-A. Roşca, D. A. Smith, D. L. Hughes and M. Bochmann, *Angew. Chem., Int. Ed.*, 2012, **51**, 10643.
8 X.-G. Xiong and P. Pyykkö, *Chem. Commun.*, 2013, **49**, 2103.
9 D.-A. Roşca, D. A. Smith and M. Bochmann, *Chem. Commun.*, 2012, **48**, 7247.
10 K. M.-C. Wong, L.-L. Hung, W. H. Lam, N. Zhu and V. W.-W. Yam, *J. Am. Chem. Soc.*, 2007, **129**, 4350.
11 For examples of electrochemical studies on (C^N^C)Au(III) pincer complexes see ref. 10 and (*a*) V. K.-M. Au, K. M.-C. Wong, N. Zhu and V. W.-W. Yam, *J. Am. Chem. Soc.*, 2009, **131**, 9076; (*b*) V. K.-M. Au, K. M.-C. Wong, D. P.-K. Tsang, M.-Y. Chan, N. Zhu and V. W.-W. Yam, *J. Am. Chem. Soc.*, 2010, **132**, 14273; (*c*) V. K.-M. Au, N. Zhu and V. W.-W. Yam, *Inorg. Chem.*, 2013, **52**, 558.
12 The reversible electrochemical oxidation of binuclear Au(I) chelate complexes to Au(II) compounds has been reported: M. Bardaj, N. G. Connelly, M. C. Gimeno, P. G. Jones, A. Laguna and M. Laguna, *J. Chem. Soc., Dalton Trans.*, 1995, 2245.
13 A small, ill-defined reduction wave at −2.09 V can also be observed as a shoulder on the main wave and likely corresponds to some trace impurity arising during the synthesis of **1**.
14 A. C. Testa and W. H. Reinmuth, *Anal. Chem.*, 1961, **33**, 1320.
15 D.-A. Roşca, J. A. Wright, D. L. Hughes and M. Bochmann, *Nat. Commun.*, 2013, **4**, 2167, DOI: 10.1038/ncomms3167.
16 The standard potentials differ from the observed reduction potentials due to the effect of the follow-up chemical steps, thus necessitating the use of digital mechanistic simulations in these more complicated cases.